Published in final edited form as:
Biomaterials. 2013 May ; 34(16): 4038–4047. doi:10.1016/j.biomaterials.2013.02.036.

The Modulation of Endothelial Cell Morphology, Function, and Survival Using Anisotropic Nanofibrillar Collagen Scaffolds

Ngan F. Huang, PhD[1,2,3], **Janet Okogbaa, BS**[1], **Jerry C. Lee, MS**[1], **Arshi Jha, MS**[1], **Tatiana S. Zaitseva, PhD**[4], **Michael V. Paukshto, PhD**[4], **John Sun, BS**[1], **Niraj Punjya**[1], **Gerald G. Fuller, PhD**[5], and **John P. Cooke, MD, PhD**[1,3,*]

[1]Division of Cardiovascular Medicine, Stanford University, Stanford, CA, USA

[2]Center for Tissue Regeneration, Repair and Restoration, Veterans Affairs Palo Alto Health Care System, 3801 Miranda Avenue, Palo Alto, CA 94304, USA

[3]The Cardiovascular Institute, Stanford, CA, USA

[4]Fibralign Corp, Sunnyvale, CA

[5]Department of Chemical Engineering, Stanford University, Stanford, CA, USA

Abstract

Endothelial cells (ECs) are aligned longitudinally under laminar flow, whereas they are polygonal and poorly aligned in regions of disturbed flow. The unaligned ECs in disturbed flow fields manifest altered function and reduced survival that promote lesion formation. We demonstrate that the alignment of the ECs may directly influence their biology, independent of fluid flow. We developed aligned nanofibrillar collagen scaffolds that mimic the structure of collagen bundles in blood vessels, and examined the effects of these materials on EC alignment, function, and *in vivo* survival. ECs cultured on 30-nm diameter aligned fibrils re-organized their F-actin along the nanofibril direction, and were 50% less adhesive for monocytes than the ECs grown on randomly oriented fibrils. After EC transplantation into both subcutaneous tissue and the ischemic hindlimb, EC viability was enhanced when ECs were cultured and implanted on aligned nanofibrillar scaffolds, in contrast to non-patterned scaffolds. ECs derived from human induced pluripotent stem cells and cultured on aligned scaffolds also persisted for over 28 days, as assessed by bioluminescence imaging, when implanted in ischemic tissue. By contrast, ECs implanted on scaffolds without nanopatterning generated no detectable bioluminescent signal by day 4 in either normal or ischemic tissues. We demonstrate that 30-nm aligned nanofibrillar collagen scaffolds guide cellular organization, modulate endothelial inflammatory response, and enhance cell survival after implantation in normal and ischemic tissues.

Keywords

collagen; cell survival; extracellular matrix; vascular grafts; endothelial cell; nanotopography

[*]ADDRESS FOR CORRESPONDENCE: John P Cooke, MD, PhD, Division of Cardiovascular Medicine, Stanford University, 300 Pasteur Drive, Stanford, CA 94305-5406, Fax Number: 650-723-8392, Telephone Number: 650-723-6459, john.cooke@stanford.edu.

1. Introduction

Endothelial cells (ECs) maintain vascular homeostasis by interacting with circulating blood components, modulating smooth muscle contractility, and providing a selective barrier to circulating small molecules and proteins [1, 2]. It is well-established that vascular ECs are elongated and aligned longitudinally along the direction of blood flow in regions of laminar flow, whereas in regions of disturbed flow the cells are polygonal and non-aligned [3]. These variations in EC morphology are accompanied by functional differences: cells exposed to disturbed flow are more prone to atherogenesis, in part due to increased expression of adhesion molecules and greater propensity for monocyte adhesion [4]. The effects of laminar flow to reduce monocyte adhesion have been assumed to be due to shear-induced release of paracrine factors such as nitric oxide from ECs, and the subsequent downregulation of adhesion molecules [5, 6]. Since laminar shear stress confers EC patterning in the presence of hemodynamic forces, it is difficult to decouple the contributions of spatial patterning and mechanical forces to EC function We therefore sought to examine the effects of spatial patterning on EC behavior and function in the absence of shear stress using extracellular matrix (ECM) nanotopography.

Besides substrate nanotopography, the chemical composition of the biomaterial also provides instructive signaling cues to cells. In particular, collagen is a major structural component of ECM in native tissues that can regulate many biological processes including cell assembly, migration, proliferation, and function [7]. Collagen is biodegradable and has low antigenicity, making it advantageous as a transplant material. Aligned collagen I fibrillar matrices were previously shown to provide essential cell-matrix interaction and guide corneal EC alignment along the fibrils [8]. However, the fibrillar matrices used in previous studies are basically an array of aligned fibrils that poorly reflects the complexity of native ECM and its mechanical properties [8, 9]. In contrast, we present the generation of aligned collagen fibrillar scaffolds with the woven-like helical and crimped configurations, which are typical for collagen-based fibrous tissue under reduced load. These aligned, woven fibrillar scaffolds better mimic the woven spiral structure of collagen bundles in relaxed blood vessels [10] and have high mechanical strength. We used a liquid collagen shearing technique to fabricate collagen membranes or scaffolds with parallel-aligned nanofibrils with controllable distribution of fibril diameters and supramolecular spatial patterns, and characterized the biological effect of anisotropic collagen nanofibrillar scaffolds on EC morphology, function, and *in vivo* survival. We hypothesized that aligned nanofibrillar collagen matrices could reorganize cytoskeletal and nuclear assembly, modulate endothelial inflammatory response, and enhance EC survival in normal and ischemic tissues.

Materials and methods

2.1 Fabrication of aligned nanofibrillar collagen substrates

The scaffold fabrication process is based on technology developed for liquid crystal display (LCD) manufacturing [11, 12] ENREF 19 ENREF 4 and is suitable for lyotropic liquid crystal materials. Purified monomeric bovine type I collagen solution was concentrated, as previously described [13-16], to reach a liquid crystal state and sheared onto glass or plastic with optical precision [17]. This method creates thin membranes with controllable fibril size, pitch, and helix diameter, as well as membrane thickness. We fabricated collagen membranes with parallel-aligned fibrils of 30 nm (FD30) and 100 nm (FD100) diameters. In addition, to examine the effect of microscale topographical cues, FD100 membranes were fabricated with an additional microgroove pattern consisting of 500-nm deep and 60-μm wide grooves arranged parallel to the fibrils (FD100-MP). Three-dimensional FD30 nanofibrillar collagen scaffolds (10 mm long and 0.18 mm in diameter) for *in vivo*

implantation were fabricated by shearing the same liquid crystal collagen solution onto a plastic substrate, delaminating the resulting membrane from the plastic, and converting the free-standing membrane into a scaffold using liquid-air surface tension [18]. The nanofibrillar materials were characterized using atomic force microscopy (AFM), diffraction patterns, and scanning electron microscopy (SEM).

2.2 Cell seeding on nanofibrillar collagen substrates

Primary human dermal microvascular endothelial cells (ECs, Lonza, passage 3-12) or human induced pluripotent stem cell-derived-ECs (iPSC-ECs, passage 8-12) ENREF 16 were cultured in EGM2-MV (Lonza) growth medium. For *in vitro* studies, nanofibrillar collagen membranes and scaffolds were sterilized in 70% ethanol and then rinsed in phosphate-buffered saline (PBS) before cell seeding at 1.3×10^4 cells/cm^2 for 7 days ($n \geq 3$). As a control substrate that does not contain ordered nanofibrillar collagen (random collagen), we coated glass substrates with 0.35 mg/mL collagen I (BD Biosciences) for cell culture.

Toward developing a nanopatterned vascular conduit, we conducted studies of bilayered scaffolds. The bilayered scaffolds consisted of 2 aligned nanofibrillar membranes with nanofibrils of the first membrane aligned orthogonal to those of the second one, for patterning both ECs and vascular smooth muscle cells (SMCs, Cell Systems, passage 18-25). These bilayered scaffolds were secured onto custom-made metal frames. ECs were seeded onto one membrane for 2 days, followed by seeding of SMCs onto the other membrane for one day. Cellular alignment was quantified by phalloidin staining for F-actin (Invitrogen) of the cytoskeleton (n=3).

2.3 EC adhesiveness on nanopatterned collagen

ECs were cultured at 1.3×10^4 cells/cm^2 for 7 days to confluency on FD30 or random collagen substrates. For monocyte adhesion assay, the ECs were stimulated with tumor necrosis factor-α (TNFα, 250 U/mL) for 7 hours. Monocytes (ATCC, U937) that were fluorescently labeled with 1,1′-dioctadecyl-3,3,3′3′-tetramethylindocarbocyanine perchlorate for 30 minwere introduced to ECs grown on either FD30 or non-patterned collagen, for 30 min under conditions of gentle shaking. Unbound cells were removed in PBS washes, and the number of monocytes in five 10X objective images were quantified and expressed as relative monocyte adhesion ($n = 3$). For quantitative PCR assessment of intercellular adhesion molecule-1 (ICAM1) and monocyte chemoattractant protein-1 (MCP1) gene expression, ECs were treated with TNFα for 24 hours, followed by cell lysis with Trizol. Quantitative PCR using Taqman primers (Applied Biosystems) were performed according to previous papers, and normalized to GAPDH housekeeping gene ($n = 3$) [19]. TNFα-treated cells were also immunofluorescently stained for ICAM1 (BD Pharmingen) and F-actin using established staining methods [20]. For quantification of ICAM1 protein expression, the mean intensity of at least 45 cells were quantified using Image J ($n = 5$).

2.4 In vivo studies

The efficacy of the FD30 substrate in maintaining cell viability in physiological and in pathological conditions was examined *in vivo*. FD30 scaffolds, 1 cm long, were pre-coated with fibronectin. Prior to implantation, human primary ECs or iPSC-ECs [21] were genetically modified with a lentiviral construct encoding firefly luciferase (FLUC) and green fluorescence protein (GFP) to confer bioluminescence and fluorescence detection, as described previously [22]. To examine the effect of aligned nanofibrillar collagen on EC survival *in vivo*, male NOD SCID (13-16 weeks old) mice received subcutaneous abdominal transplants of FD30 collagen scaffold, 4×10^3 ECs in Dulbecco's Modified Eagle's Medium (DMEM), 4×10^3 ECs cultured on the FD30 scaffold, or 4×10^3 ECs cultured on a non-

patterned scaffold (NP1, Plain catgut collagen, Aspide Sutures) ($n = 4$). Cell survival was tracked by bioluminescence imaging (BLI) for up to 14 days [21]. For assessing cell survival in an ischemic disease model, we induced unilateral hindlimb ischemia by excising the femoral artery, as previously described [23]. The animals were randomized to receive the FD30 scaffold seeded with 4×10^3 ECs, NP1 scaffold seeded with 4×10^3 ECs, another non-patterned scaffold (NP2, 3-0 plain gut collagen sutures, Ethicon) seeded with 4×10^3 ECs, or 4×10^3 cells in 30 μl PBS into the adductor muscle ($n > 5$). The scaffolds were implanted and sutured adjacent to the site of femoral artery excision. Immediately prior to BLI, the animals were injected intraperitoneally with D-luciferin (375 mg/kg body weight). For up to 2 weeks, cell viability was tracked by BLI. Similar hindlimb ischemia studies were performed using iPSC-ECs and examined using BLI for up to 4 weeks ($n = 6$). All animal experiments were performed with approval by the Administrative Panel on Laboratory Animal Care in Stanford University.

2.5 Statistical analysis

All data are shown as mean ± standard deviation. Statistical comparisons between 2 groups were quantified by a *t*-test. For comparisons of 3 or more groups, ANOVA with Holm's adjustment for multiple comparisons was used. A Repeated Measures ANOVA with Holm's adjustment was used for comparisons of the same samples over time. Statistical significance was accepted at $p < 0.05$.

3. Results

3.1 Characterization of aligned membranes and scaffolds

Using liquid shearing technique, we fabricated nanofibrillar membranes having helical-like fibrils with three different arrangements (FD30, FD100 and FD100-MP), deposited on glass substrates. AFM analysis of the FD100 membrane shows a nematic structure with highly aligned ~100 nm collagen fibrils (Fig. 1A). The FD30 membrane has an additional translational order formed by the peaks of helices of the helical-like 30-nm fibrils ("crimp") [16]. ENREF 24 ENREF 29 ENREF 25 This crimp is perpendicular to the direction of fibril alignment (Fig. 1B). Collectively, crimps form the "crimp pattern." The difference between the two structures is related to the difference in ionic strength of the initial collagen solution. The structures in Fig. 1A-B correspond to collagen solution conductivities about 4 and 7.8 mS, respectively. The woven-like helical and crimped configurations of collagen fibrils (Fig. 1A-B) are typical for collagen-based fibrous tissue when external load is reduced, and mimic the woven spiral structure of collagen bundles in relaxed blood vessels [10]. The woven-like helical configuration of 100-nm fibrils (FD100) was also supplemented with a microgroove pattern consisting of 500-nm deep and 60-μm wide grooves arranged parallel to the fibrils (FD100-MP), as shown by AFM analysis (Fig. 1C). Corresponding SEM images of the aligned pattern of collagen fibrils and the microgrooves are shown in Fig. 1D-1F. All glass substrates were uniformly covered with the collagen fibrils. Diffraction patterns further verified the orientation of nanofibrils (Supplementary Fig.1).

3.2 Modulation of EC alignment on aligned collagen nanofibrils

Primary human ECs, SMCs, or fibroblasts were cultured on aligned nanofibrillar collagen membranes. In our initial studies we utilized FD100 or FD100-MP. Although human SMCs or fibroblasts aligned well on this material (Supplementary Fig. 2 & 3), to our disappointment, we did not observe alignment of ECs grown on these substrates. Subsequently, we used smaller diameter fibrils 30 nm (FD30), with the hypothesis that ECs may sense and respond to smaller architectural elements. To examine the effect of nanotopographical features on cytoskeletal assembly, we fluorescently stained for cytoskeletal F-actin fibers using phalloidin. Fluorescence microscopy revealed dramatic

effects on cellular orientation induced by these modified substrates (Fig. 2A-D). After 4 days of cell culture, ECs on FD30 and FD100 substrates had significantly organized F-actin assembly that were 9 ± 2° or 19 ± 8° along the nanofibr il direction, respectively, whereas cells cultured on the control substrates had F-actin fibers randomly distributed within 49 ± 3° with respect to an arbit rary axis ($p < 0.0001$, Fig. 2G; in this analysis, a value of 45° represents entirely random orientation of axis of cultured cells). The addition of microgrooves appeared to reverse the effect of 100-nm fibrils on cell guidance, as samples on the FD100-MP samples were not significantly different from the control substrates on day 4. After 7 days when the cells were confluent, cells on FD30 and FD100 substrates remained significantly aligned, in comparison to the control substrate (9 ± 2° FD30 and 23 ± 5° FD100 vs 48 ± 6° control, $p < 0.0001$, Fig. 2G). The cells on FD30 were notably elongated in morphology, in comparison to the ECs on the control substrates which had larger cell area and “cobble-stone” morphology, as shown by SEM (Fig. 2E-F). By 7 days, the cells cultured on the FD100-MP samples showed modest effect in cellular alignment (38 ± 1°) that was significantly different from that of the control substrate ($p < 0.014$).

As an additional method for quantification of F-actin assembly, we used automated two-dimensional Fast Fourier Transform (FFT) analysis to generate frequency plots and alignment histograms. The frequency plots depict random orientation as pixels evenly distributed about the origin, and parallel alignment as pixels organized along the axis of the nanofibrils. In this analysis, the frequency plots depict distinct organization of pixels along the fiber axis on the FD30 samples (Fig. 2H **inset**), whereas the control substrates are represented by pixels evenly distributed about the origin. The frequency plots were also displayed as frequency alignment histograms that depict the principal angle of orientation within 360° of space (Fig. 2H). Based on FFT analysis, the alignment on control substrates consists of low frequency peaks with a Gaussian distribution that is commonly observed in randomly oriented assemblies. In contrast, the alignment histograms for the FD30 substrate showed 2 distinctive peaks separated by 180°, concurring with cell align ment analysis (Fig. 2G) that the cells primarily align along the same direction. Therefore, both the FFT (Fig. 2H) and cellular alignment (Fig. 2G) analyses show that FD30 substrates promote EC alignment along the direction of collagen nanofibrils.

3.3 Modulation of nuclear alignment on aligned collagen nanofibrils

Besides modulating the actin cytoskeleton, the aligned nanofibrillar substrates also affected nuclear elongation as revealed by the nuclear shape index (NSI), which was defined as $(4\pi * \text{Area})/(\text{Perimeter}^2)$, in which a value of 1 approximated the shape of a circle and a value of 0 depicted that of a straight line [24]. As ECs became progressively more aligned along the direction of the nanofibrils from the FD100-MP to FD30 substrates, the NSI significantly decreased, suggesting that the nuclei became increasingly more elongated (Supplementary Fig. 4C, $p < 0.001$). Similar reduction in NSI was also observed in SMCs and fibroblasts when comparing the nanopatterned collagen fibrils to the control substrates (Supplementary Fig. 4A-B). Together, these results suggest that aligned nanofibrillar collagen substrates could modulate F-actin assembly and nuclear elongation.

3.4 Modulation of EC inflammatory properties on aligned collagen nanofibrils

It is well established that laminar shear stress modulates both endothelial function and morphology. ECs exposed to laminar blood flow in a straight segment of an artery are aligned longitudinally along the direction of blood flow, and aligned ECs are less adhesive for monocyte attachment [4]. To determine if nanofibril-induced cellular alignment could also confer similar functional effects, we cultured ECs on either the FD30 or control substrates to confluency. ECs that were aligned on FD30 substrates or non-aligned on the control substrates were then exposed to the inflammatory cytokine, TNFα, followed by the

incubation of the ECs with fluorescently labeled monocytes. Notably, for the ECs grown on FD30 collagen, there was a 50% reduction in the numbers of adherent monocytes by comparison to the ECs grown on random collagen (Fig. 3 A,C). To further verify these results, we next interrogated the expression of adhesion markers and chemokines that may account for the reduction in monocyte adhesion. Indeed, ICAM1 was significantly reduced in cells cultured on the aligned nanofibrillar substrate at the protein (Fig. 3 B,D) and gene expression (Fig. 3E) levels, in comparison to cells cultured on the non-patterned substrate. Furthermore, MCP-1 gene expression was also significantly reduced on the aligned nanopatterned substrate. These results are consistent with reduced EC adhesiveness on the FD30 substrate, leading to reduced monocyte adhesion. Together, these results suggest that, even in the absence of shear stress, nanofibril-induced EC alignment could modulate EC adhesiveness.

To exclude the possibility of cytotoxicity or reduced proliferation as causes for reduced monocyte adhesion, we used a Live/Dead cytotoxicity assay and immunofluorescence staining of cell cycle marker, Ki67. All three cell types showed robust calcein AM uptake (green), suggesting high cell viability on all of the collagen configurations (Supplementary Fig. 5). Proliferation analysis based on the cell cycle marker, Ki67, demonstrated that fibroblasts and SMCs generally showed a decline in proliferation from 4 to 7 days, presumably due to cell contact inhibition, without any significant difference between the various substrates at the same time point (Supplementary Fig. 6). For ECs, there was only a modest increase in proliferation on day 7 on the FD100 substrate, when compared to the other substrates ($p < 0.04$). These data suggest that F30 substrates could modulate inflammatory response of ECs.

3.5 EC survival upon subcutaneous implantation on aligned nanofibrillar scaffolds

In addition to evaluating endothelial morphology and function *in vitro*, we assessed whether aligned FD30 nanofibrillar collagen scaffolds could enhance the survival of implanted ECs under physiological or pathophysiological conditions. Human ECs in an aligned flow field have a longer lifetime than those in a disturbed flow field. For example, ECs in the disturbed flow field at the iliac artery bifurcation manifest shorter telomeres, an indication of more frequent cell turnover in these zones [25]. Accordingly, in addition to evaluating endothelial morphology and function *in vitro*, we assessed whether aligned FD30 nanofibrillar collagen scaffolds could enhance the survival of implanted ECs under physiological or pathophysiological conditions. The nanofibrillar FD30 matrix was fabricated into three-dimensional porous scaffolds and then characterized for mechanical properties. Uniaxial tension tests for the collagen scaffold with cross-section 1.2 μm × 25000 μm (~180 μm effective diameter) showed that its maximum load was 2.1 N in dry state, 0.9 N in wet state, and its elastic modulus was 160 ± 20 MPa. These mechanical properties are consistent with collagen materials with high mechanical strength.

We cultured ECs on FD30 nanofibrillar scaffolds. Based on SEM microscopy, the ECs were generally aligned longitudinally along the direction of the nanofibrils (Fig. 4A-B). The ECs maintained robust expression of the endothelial specific marker CD31 (Fig. 4C) and proliferation antigen Ki67 (Fig. 4D), suggesting that the cells maintained their phenotype and proliferated on the scaffold. Each scaffold contained ~4000 cells, as quantified by dissociation of the cells from the graft after confluent cell attachment.

We investigated the ability of aligned nanofibrillar scaffolds as cell delivery vehicles to maintain cell viability upon transplantation. To enable non-invasive imaging of the transplanted ECs by BLI and fluorescence microscopy, we genetically modified the cells with a lentiviral construct and purified the cells that were transduced based on GFP expression (Supplementary Fig. 7A-B). This genetic modification did not affect cell

behavior as the ECs maintained expression of endothelial markers such as CD31 while also expressing GFP (Supplementary Fig. 7C). The transduced cells were indeed bioluminescent, and the bioluminescence intensity correlated linearly with cell numbers, and this relationship enabled quantification of cell density non-invasively *in vivo* (Supplementary Fig. 7D-E).

To examine the effect of aligned nanofibrillar collagen on EC survival, male NOD SCID mice received subcutaneous abdominal transplants of 1) FD30 collagen scaffold, 2) 4×10^3 ECs in DMEM, 3) 4×10^3 ECs cultured on the FD30 scaffold, or 4) 4×10^3 ECs cultured on a non-patterned (NP1) scaffold (Supplementary Fig. 8, $n = 4$). Using BLI to track cell survival and localization in subcutaneous implants, we demonstrated that the EC-seeded scaffolds showed prolonged survival for at least 14 days, with an average in bioluminescence intensity of $3.7 \pm 3.4 \times 10^5$ $ps^{-1}cm^{-2}sr^{-1}$ on day 0 and $1.1 \pm 1.7 \times 10^6$ $ps^{-1}cm^{-2}sr^{-1}$ on day 14 (Fig. 5 A-B). In stark contrast, when similar numbers of cells were delivered on the NP1 scaffold or injected in media alone, cell survival rapidly declined and the bioluminescence signal was no longer detectable over the threshold after 4 days. The acellular scaffold group demonstrated no detectable signal besides for endogenous background that was below threshold. These data indicated that the FD30 scaffold supported cell survival and localization to the transplant site for at least 14 days, whereas cells delivered on either the control NP1 scaffold or in media were no longer viable or were cleared from the region of implantation within 4 days.

3.6 EC cell survival on aligned nanofibrillar scaffolds upon implantation into the ischemic hindlimb

Based on the finding of enhanced EC cell survival in non-diseased subcutaneous tissue, we next examined whether aligned FD30 nanofibrillar scaffolds could also maintain cell survival in the hostile environment of an ischemic tissue, where death of implanted cells is increased due to hypoxia, inflammation, and reduced nutrient availability. Upon induction of hindlimb ischemia by excision of the femoral artery, we transplanted in the bed of the excised femoral artery one of the following: 1) 4×10^3 ECs cultured on the FD30 scaffolds, 2) 4×10^3 ECs cultured on the NP1 scaffold, or 3) 4×10^3 ECs in saline. Notably, the cells on the FD30 scaffolds survived for up to 14 days, although there was gradual decrease in bioluminescence intensity from day 1 ($2.3 \pm 3.6 \times 10^5 ps^{-1}cm^{-2}sr^{-1}$) to day 14 ($4.1 \pm 7.5 \times 10^4$ $ps^{-1}cm^{-2}sr^{-1}$) (Fig. 6A-B), which could be attributed to the ischemic environment. In contrast, the cells delivered in saline showed a rapid decrease in signal by day 1 post-transplantation ($1.8 \pm 1.4 \times 10^4$ $ps^{-1}cm^{-2}sr^{-1}$) and were undetectable by day 4. To our surprise, cell survival on the NP1 scaffold was also very low after day 1 ($2.2 \pm 1.4 \times 10^4$ $ps^{-1}cm^{-2}sr^{-1}$) and below the threshold for a positive signal by day 4. We confirmed these results using another non-patterned scaffold (NP2), showing again that cell survival on non-patterned scaffold in the ischemic hindlimb setting was low and no longer detectable within 4 days (Supplementary Fig 9). This data suggested that the FD30 scaffold promoted cell survival under ischemic conditions for at least 14 days, whereas the non-patterned control scaffolds could not maintain cell survival for more than 4 days.

To further validate this finding, we performed *in vitro* studies to quantify cell death under conditions mimicking ischemia (hypoxia and reduced nutrient conditions) for 24 hours. Under the conditions of 1% O_2 and 5% FBS without additional growth factors, the relative level of non-viable cells was more than 2-fold higher on the NP2 scaffold than when compared to the FD30 scaffold, based on the intensity of ethidium homodimer fluorescent dye that labels non-viable cell nuclei (Supplementary Fig. 10). Confirmation of the increased cell death on the non-patterned control scaffold in these *in vitro* studies corroborated our *in vivo* results suggesting that the FD30 scaffold could more effectively promote cell viability.

To determine whether the aligned collagen scaffold could also maintain cell survival of another type of EC, namely human induced pluripotent stem cell-derived ECs (iPSC-ECs), we delivered iPSC-EC-seeded FD30 scaffolds into the ischemic limb. Previously, we reported that a single injection of iPSC-ECs (5×10^5 cells) in saline into the ischemic hindlimb were no longer detectable after 11 days using BLI [21]. Notably, despite starting with fewer cells (by two orders of magnitude) we could detect a bioluminescence signal from cells on the scaffold *in vivo* for at least 28 days. When a similar number (4×10^3) of iPSC-ECs were injected in saline, they disappeared by 4 days (Supplementary Fig. 11, 12). These findings suggest that cell delivery on nanofibrillar collagen scaffolds could promote prolonged cell survival in ischemic tissues.

3.7 Bilayered membranes for EC and SMC coculture

Based on our findings of nanotopography-mediated effects on promoting EC alignment and anti-inflammatory function, a potential therapeutic device is a bilayered vascular graft consisting of a luminal layer of aligned collagen nanofibrils oriented longitudinally along the direction of blood flow to guide endothelial alignment and an outer layer containing circumferentially oriented nanofibrils to guide the assembly of SMCs (Fig. 7A). To mimic the orthogonal alignment of cells between the intimal and medial layers, we constructed bilayered membranes consisting of an FD30 upper membrane to guide the assembly of ECs and a FD100 lower membrane for SMC culture. The nanofibrils of the two membranes were oriented orthogonal to one another to mimic their physiological orientation (Fig. 7B). As shown in Fig. 7C, the bilayered membranes were secured in metal frames for sequential seeding of ECs and then SMCs. After 3 days of culture, we quantified cell alignment by staining for F-actin using phalloidin. Fig. 7D demonstrates the orthogonal alignment of ECs and SMCs that match their orthogonal alignment in vivo. Cellular alignment of the ECs and SMCs were within 15 degrees from the axis of the nanofibrils (Fig. 7E), which represents highly aligned cells. This data suggests that nanotopographical cues may be beneficial for guiding cellular alignment and function in engineered vascular conduits.

4. Discussion

The salient findings of this work are: 1) by comparison to human SMCs and fibroblasts, human ECs are more sensitive to the fibril size of aligned collagen matrices, aligning best on collagen nanofibrils with smaller features (Fig. 2, Supplementary Fig. 2 & 3); 2) aligned collagen nanofibrils (FD30) could efficiently guide cytoskeletal assembly and nuclear orientation of ECs (Fig. 2, Supplementary Fig. 4); 3) aligned ECs cultured on FD30 substrates were less adhesive for monocytes (Fig. 3), suggesting that biological properties of the ECs could be regulated by alignment; 4) aligned FD30 scaffolds could promote EC survival and retention in both non-ischemic and ischemic tissues for up to 28 days (Figs. 5, 6, Supplementary Fig. 12).

Our findings indicate that the alignment of ECs *per se*, independent of shear stress, can favorably modify endothelial biology. Based on the nanotopography-mediated effects on EC morphology and function demonstrated in this study, we envision several venues for developing our aligned collagen scaffolds into therapeutic devices. First it could be a bilayered vascular graft consisting of a luminal layer of aligned collagen nanofibrils oriented longitudinally along the direction of blood flow to guide endothelial alignment and an outer layer containing circumferentially oriented nanofibrils to guide the assembly of SMCs. The proposed bilayered construct could promote a physiologically relevant alignment pattern of ECs and SMCs (Fig. 7). Furthermore, based on our monocyte adhesion studies demonstrating reduced adhesion on aligned nanofibrils (Fig. 3), this anisotropic vascular graft may be more resistant to atherogenesis or myointimal hyperplasia compared to isotropic grafts.

In addition, using our scaffold as cell delivery device could be beneficial for cell therapy approach. Currently, a major limitation in the efficacy of cell-based therapies is donor cell loss, especially upon transplantion into sites of tissue damage. Cell survival can be promoted by small molecules or target gene activation [26-28], and it may be further improved by providing appropriate ECM microenvironmental cues. In addition to providing a scaffolding support, the ECM imparts instructive cues to the cell, activating cell signaling pathways that can trigger biological responses such as migration, proliferation, and survival [29, 30]. Recent data showed that scaffold in form of fibrin microthreads support hMSC viability and proliferation and suggested it could improve localized cell delivery [31]. In line with these data, we demonstrated that when cells were pre-seeded onto the FD30 scaffold before transplantation, the scaffold could serve as a cell delivery vehicle that provides site-specific cell retention and survival. In contrast to the non-patterned scaffolds that lack specific topographical features, the FD30 scaffolds may provide instructive nano- and microtopographical cues that promote cell survival. Other additional advantages of aligned nanofibrillar scaffolds include as tunable mechanicaland degradation properties, scalability in fabrication, and ease in control over fibril diameters.

We showed that aligned nanofibrillar collagen could modulate not only morphological changes in ECs, but also their functional modes in inflammatory response and cell survival. The mechanism by which nanotopography confers cues that direct cellular behavior is thought to be related to cryptic binding sites on ECMs that become revealed as a result of nanotopography-mediated cellular forces [32-34]. ENREF 19 Our finding is consistent with a larger body of literature suggesting that nanoscale topographies trigger signal transduction pathways, presumably by activating cell surface integrin receptors and focal adhesions that relay cues from the ECM to the cytoskeleton [35-37].

With the recognition of scaffold architecture as a critical factor in tissue engineering, the scaffold design has evolved from isotropic to anisotropic, more complex biomimetic scaffolds, with the goal being to simulate the ECM architecture of specific tissues and to influence the organization and function of target cells. Collagen, being the main natural ECM component, may be an ideal choice for an engineered scaffold material, as it has the advantage of providing both structural and microenviromental support, the latter through storage and delivery of biologically active factors. Moreover, collagen I scaffolds are biodegradable and low in antigenicity, making them suitable for transplantation. Current laboratory methods aimed at achieving orientational anisotropy in reconstituted collagen matrices include mechanical loading [38], microfluidic alignment [39, 40], flow and magnetic field induced alignment [41], electrochemical processing [42], interstitial flow [43], high magnetic field [44, 45], oriented electrospinning [46], Langmuir-Blodgett deposition [47], extrusion processes [48, 49], and spin-coating [50]. Aligned collagen I matrices produced by these methods provided for essential cell-matrix interaction and successfully guided fibroblast [51-53] and endothelial cell alignment [8]. However, these matrices are essentially two-dimensional in structure [8] and lack secondary structures that mimic the spatial complexity of natural ECMs [54] such as crimps [55] and microscale topographical features. The lack of secondary structure results in poor strength of the synthetic scaffold and affects cellular survival and behavior [56, 57]. To overcome these challenges, we developed a production process to fabricate bioequivalent scaffolds with controlled three-dimensional nano- and micro-structure, pre-determined thickness, fibril size, and high uniformity. These scaffolds 1) better mimic the complexity of native ECM at nano- and micro-scales, 2) show high mechanical strength, 3) have uniform properties over a large area of several cm^2, and 4) have controlled biodegradation rate depending on the level of crosslinking. Furthermore, these scaffolds provide a high degree of cell adhesion and confer cell guidance signals. We anticipate these materials will have translational applications for tissue engineering and regenerative medicine.

5. Conclusion

In summary, this study demonstrates the capacity of anisotropic nanofibrillar collagen to organize cytoskeletal and nuclear components of ECs, and to favorably influence inflammation and cell viability *in vivo*. The collagen scaffolds with aligned 30-nm diameter fibrils could orient F-actin stress fiber assembly in ECs along the nanofibril direction and promote reduced adhesiveness for monocytes, when compared to isotropic non-fibrillar collagen substrates. Cell survival after implantation into normal or ischemic hindlimb tissue was markedly prolonged when ECs were cultured and implanted on the aligned nanofibrillar scaffolds, in comparison to randomly oriented scaffolds. We further demonstrated similar improvement in cell viability after implantation of the aligned scaffolds seeded with iPSC-ECs. This work highlights the importance of nanotopography for therapeutic cell delivery and presents a new approach to enhance cell survival *in vivo*.

Supplementary Material

Refer to Web version on PubMed Central for supplementary material.

Acknowledgments

The authors are very grateful to Yu. Bobrov (NT-MDT) for the skilled assistance with AFM imaging and processing. This study was supported by grants from National Institutes of Health to JPC (U01HL10039, RC2HL103400,1K12HL087746) and NFH (HL098688), and the US Army Medical Research and Materiel Command (W81XWH-12-C-0111) to MVP.

REFERENCES

[1]. Gimbrone MA Jr. Nagel T, Topper JN. Biomechanical activation: An emerging paradigm in endothelial adhesion biology. J Clin Invest. 1997; 100(11 Suppl):S61–65. [PubMed: 9413404]

[2]. Gimbrone MA Jr. Topper JN, Nagel T, Anderson KR, Garcia-Cardena G. Endothelial dysfunction, hemodynamic forces, and atherogenesis. Ann N Y Acad Sci. 2000; 902:230–239. discussion 239-240. [PubMed: 10865843]

[3]. Chien S. Effects of disturbed flow on endothelial cells. Ann Biomed Eng. 2008; 36(4):554–562. [PubMed: 18172767]

[4]. Cooke JP. Flow, no, and atherogenesis. Proc Natl Acad Sci U S A. 2003; 100(3):768–770. [PubMed: 12552094]

[5]. Tsao PS, Buitrago R, Chan JR, Cooke JP. Fluid flow inhibits endothelial adhesiveness. Nitric oxide and transcriptional regulation of vcam-1. Circulation. 1996; 94(7):1682–1689. [PubMed: 8840861]

[6]. Tsao PS, Lewis NP, Alpert S, Cooke JP. Exposure to shear stress alters endothelial adhesiveness. Role of nitric oxide. Circulation. 1995; 92(12):3513–3519. [PubMed: 8521574]

[7]. Egeblad M, Rasch MG, Weaver VM. Dynamic interplay between the collagen scaffold and tumor evolution. Curr Opin Cell Biol. 2010; 22(5):697–706. [PubMed: 20822891]

[8]. Gruschwitz R, Friedrichs J, Valtink M, Franz CM, Muller DJ, Funk RH, et al. Alignment and cell-matrix interactions of human corneal endothelial cells on nanostructured collagen type i matrices. Invest Ophthalmol Vis Sci. 2010; 51(12):6303–6310. [PubMed: 20631237]

[9]. Bouta EM, McCarthy CW, Keim A, Wang HB, Gilbert RJ, Goldman J. Biomaterial guides for lymphatic endothelial cell alignment and migration. Acta Biomater. 2011; 7(3):1104–1113. [PubMed: 20974299]

[10]. Arkill KP, Moger J, Winlove CP. The structure and mechanical properties of collecting lymphatic vessels: An investigation using multimodal nonlinear microscopy. J Anat. 2010; 216(5):547–555. [PubMed: 20345855]

[11]. Paukshto M, Fuller G, Michailov A, Remizov S. Optics of sheared liquid-crystal polarizer based on aqueous dispersion of dichroic-dye nano-aggregates. J Soc Inf Display. 2005; 13:765–772.

[12]. Ukai Y, Ohyama T, Fennell L, Kato Y, Paukshto M, Smith P, et al. Current status and future prospect of in-cell polarizer technology. SID Symposium Digest. 2004; 35:1170–1173.

[13]. Kirkwood JE, Fuller GG. Liquid crystalline collagen: A self-assembled morphology for the orientation of mammalian cells. Langmuir. 2009; 25(5):3200–3206. [PubMed: 19437784]

[14]. Paukshto M, McMurtry D, Bobrov Y, Sabelman E. Oriented collagen-based materials, films and methods of making same. World Intellectual Property Organization 2008. WO/2008/131293.

[15]. Bobrov Y, Fennell L, Lazarev P, Paukshto M, Remizov S. Manufacturing of a thin-film lcd. J Soc Inf Display. 2002; 10:317–321.

[16]. Muthusubramaniam L, Peng L, Zaitseva T, Paukshto M, Martin GR, Desai TA. Collagen fibril diameter and alignment promote the quiescent keratocyte phenotype. J Biomed Mater Res A. 2012; 100(3):613–621. [PubMed: 22213336]

[17]. McMurtry D, Paukshto M, Bobrov Y. A liquid film applicator assembly and rectilinear shearing system incorporating the same. World Intellectual Property Organization 2008. WO/2008/063631.

[18]. Paukshto MV, McMurtry DH, Martin GR, Zaitseva T, Bobrov YA. Biocomposites and methods of making the same. World Intellectual Property Organization 2010. WO/2010/019625.

[19]. Huang NF, Fleissner F, Sun J, Cooke JP. Role of nitric oxide signaling in endothelial differentiation of embryonic stem cells. Stem Cells Dev. 2010; 19(10):1617–1626. [PubMed: 20064011]

[20]. Huang NF, Patel S, Thakar RG, Wu J, Hsiao BS, Chu B, et al. Myotube assembly on nanofibrous and micropatterned polymers. Nano Lett. 2006; 6(3):537–542. [PubMed: 16522058]

[21]. Rufaihah AJ, Huang NF, Jame S, Lee JC, Nguyen HN, Byers B, et al. Endothelial cells derived from human ipscs increase capillary density and improve perfusion in a mouse model of peripheral arterial disease. Arterioscler Thromb Vasc Biol. 2011; 31(11):e72–79. [PubMed: 21836062]

[22]. Huang NF, Niiyama H, Peter C, De A, Natkunam Y, Fleissner F, et al. Embryonic stem cell-derived endothelial cells engraft into the ischemic hindlimb and restore perfusion. Arterioscler Thromb Vasc Biol. 2010; 30(5):984–991. [PubMed: 20167654]

[23]. Niiyama H, Huang NF, Rollins MD, Cooke JP. Murine model of hindlimb ischemia. J Vis Exp. 2009; 23:1035. [PubMed: 19229179]

[24]. Aubin H, Nichol JW, Hutson CB, Bae H, Sieminski AL, Cropek DM, et al. Directed 3d cell alignment and elongation in microengineered hydrogels. Biomaterials. 2010; 31(27):6941–6951. [PubMed: 20638973]

[25]. Chang E, Harley CB. Telomere length and replicative aging in human vascular tissues. Proc Natl Acad Sci U S A. 1995; 92(24):11190–11194. [PubMed: 7479963]

[26]. Gnecchi M, He H, Noiseux N, Liang OD, Zhang L, Morello F, et al. Evidence supporting paracrine hypothesis for akt-modified mesenchymal stem cell-mediated cardiac protection and functional improvement. FASEB J. 2006; 20(6):661–669. [PubMed: 16581974]

[27]. Li W, Ma N, Ong LL, Nesselmann C, Klopsch C, Ladilov Y, et al. Bcl-2 engineered mscs inhibited apoptosis and improved heart function. Stem Cells. 2007; 25(8):2118–2127. [PubMed: 17478584]

[28]. Pons J, Huang Y, Arakawa-Hoyt J, Washko D, Takagawa J, Ye J, et al. Vegf improves survival of mesenchymal stem cells in infarcted hearts. Biochem Biophys Res Commun. 2008; 376(2): 419–422. [PubMed: 18789891]

[29]. Daley WP, Peters SB, Larsen M. Extracellular matrix dynamics in development and regenerative medicine. J Cell Sci. 2008; 121(Pt 3):255–264. [PubMed: 18216330]

[30]. Huang NF, Li S. Regulation of the matrix microenvironment for stem cell engineering and regenerative medicine. Ann Biomed Eng. 2011; 39(4):1201–1214. [PubMed: 21424849]

[31]. Proulx MK, Carey SP, Ditroia LM, Jones CM, Fakharzadeh M, Guyette JP, et al. Fibrin microthreads support mesenchymal stem cell growth while maintaining differentiation potential. J Biomed Mater Res A. 2011; 96(2):301–312. [PubMed: 21171149]

[32]. Smith ML, Gourdon D, Little WC, Kubow KE, Eguiluz RA, Luna-Morris S, et al. Force-induced unfolding of fibronectin in the extracellular matrix of living cells. PLoS Biol. 2007; 5(10):e268. [PubMed: 17914904]

[33]. Garcia AJ, Vega MD, Boettiger D. Modulation of cell proliferation and differentiation through substrate-dependent changes in fibronectin conformation. Mol Biol Cell. 1999; 10(3):785–798. [PubMed: 10069818]

[34]. Teo BK, Ankam S, Chan LY, Yim EK. Nanotopography/mechanical induction of stem-cell differentiation. Methods Cell Biol. 2010; 98:241–294. [PubMed: 20816238]

[35]. Dalby MJ, Childs S, Riehle MO, Johnstone HJ, Affrossman S, Curtis AS. Fibroblast reaction to island topography: Changes in cytoskeleton and morphology with time. Biomaterials. 2003; 24(6):927–935. [PubMed: 12504513]

[36]. Geiger B, Spatz JP, Bershadsky AD. Environmental sensing through focal adhesions. Nat Rev Mol Cell Biol. 2009; 10(1):21–33. [PubMed: 19197329]

[37]. Geiger B, Bershadsky A, Pankov R, Yamada KM. Transmembrane crosstalk between the extracellular matrix--cytoskeleton crosstalk. Nat Rev Mol Cell Biol. 2001; 2(11):793–805. [PubMed: 11715046]

[38]. Sellaro TL, Hildebrand D, Lu Q, Vyavahare N, Scott M, Sacks MS. Effects of collagen fiber orientation on the response of biologically derived soft tissue biomaterials to cyclic loading. J Biomed Mater Res A. 2007; 80(1):194–205. [PubMed: 17041913]

[39]. Lee P, Lin R, Moon J, Lee LP. Microfluidic alignment of collagen fibers for in vitro cell culture. Biomed Microdevices. 2006; 8(1):35–41. [PubMed: 16491329]

[40]. Lanfer B, Freudenberg U, Zimmermann R, Stamov D, Korber V, Werner C. Aligned fibrillar collagen matrices obtained by shear flow deposition. Biomaterials. 2008; 29(28):3888–3895. [PubMed: 18606448]

[41]. Guo C, Kaufman LJ. Flow and magnetic field induced collagen alignment. Biomaterials. 2007; 28(6):1105–1114. [PubMed: 17112582]

[42]. Cheng X, Gurkan UA, Dehen CJ, Tate MP, Hillhouse HW, Simpson GJ, et al. An electrochemical fabrication process for the assembly of anisotropically oriented collagen bundles. Biomaterials. 2008; 29(22):3278–3288. [PubMed: 18472155]

[43]. Ng CP, Swartz MA. Mechanisms of interstitial flow-induced remodeling of fibroblast-collagen cultures. Ann Biomed Eng. 2006; 34(3):446–454. [PubMed: 16482410]

[44]. Torbet J, Ronziere MC. Magnetic alignment of collagen during self-assembly. Biochem J. 1984; 219(3):1057–1059. [PubMed: 6743242]

[45]. Guido S, Tranquillo RT. A methodology for the systematic and quantitative study of cell contact guidance in oriented collagen gels. Correlation of fibroblast orientation and gel birefringence. J Cell Sci. 1993; 105(Pt 2):317–331. [PubMed: 8408268]

[46]. Zhong S, Teo WE, Zhu X, Beuerman RW, Ramakrishna S, Yung LY. An aligned nanofibrous collagen scaffold by electrospinning and its effects on in vitro fibroblast culture. J Biomed Mater Res A. 2006; 79(3):456–463. [PubMed: 16752400]

[47]. Goffin AJ, Rajadas J, Fuller GG. Interfacial flow processing of collagen. Langmuir. 2010; 26(5): 3514–3521. [PubMed: 20000428]

[48]. Evans HJ, Sweet JK, Price RL, Yost M, Goodwin RL. Novel 3d culture system for study of cardiac myocyte development. Am J Physiol Heart Circ Physiol. 2003; 285(2):H570–578. [PubMed: 12730055]

[49]. Lai ES, Anderson CM, Fuller GG. Designing a tubular matrix of oriented collagen fibrils for tissue engineering. Acta Biomater. 2011; 7(6):2448–2456. [PubMed: 21414424]

[50]. Saeidi N, Sander EA, Zareian R, Ruberti JW. Production of highly aligned collagen lamellae by combining shear force and thin film confinement. Acta Biomater. 2011; 7(6):2437–2447. [PubMed: 21362500]

[51]. Friedrichs J, Taubenberger A, Franz CM, Muller DJ. Cellular remodelling of individual collagen fibrils visualized by time-lapse afm. J Mol Biol. 2007; 372(3):594–607. [PubMed: 17686490]

[52]. Heino J. The collagen receptor integrins have distinct ligand recognition and signaling functions. Matrix Biol. 2000; 19(4):319–323. [PubMed: 10963992]

[53]. Poole K, Khairy K, Friedrichs J, Franz C, Cisneros DA, Howard J, et al. Molecular-scale topographic cues induce the orientation and directional movement of fibroblasts on two-dimensional collagen surfaces. J Mol Biol. 2005; 349(2):380–386. [PubMed: 15890202]

[54]. Lutolf MP, Hubbell JA. Synthetic biomaterials as instructive extracellular microenvironments for morphogenesis in tissue engineering. Nat Biotechnol. 2005; 23(1):47–55. [PubMed: 15637621]

[55]. Silver, FH. Mechanosensing and mechanochemical transduction in extracellular matrix: Biological, chemical, engineering, and physiological aspects. Springer; New York: 2006.

[56]. Badylak SF. The extracellular matrix as a biologic scaffold material. Biomaterials. 2007; 28(25): 3587–3593. [PubMed: 17524477]

[57]. Schussler O, Chachques JC, Mesana TG, Suuronen EJ, Lecarpentier Y, Ruel M. 3-dimensional structures to enhance cell therapy and engineer contractile tissue. Asian Cardiovascular & Thoracic Annals. 2010; 18(2):188–198. [PubMed: 20304859]

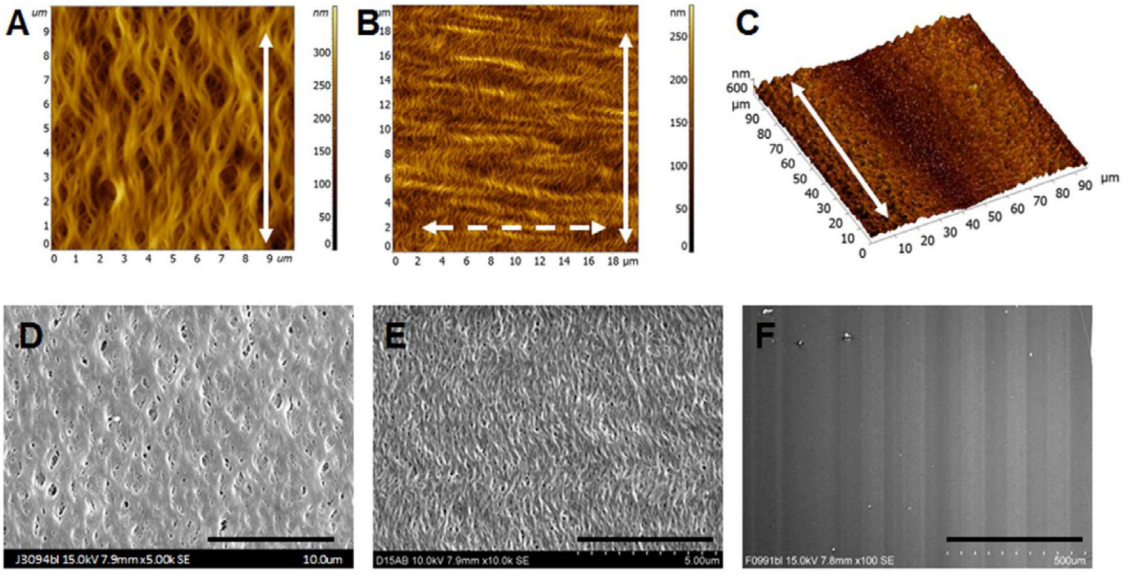

Fig. 1. Characterization of the nanofibrillar collagen membranes

Characterization of the fibril diameter (A, 100 nm; B, 30 nm) and microgroove size (C, 60-μm wide microgrooves and 100 nm fibrils) by atomic force microscopy. Solid arrow shows the direction of the fibrils, and dashed arrow shows the direction of the crimp. Visualization of crimped fibrils (D, 100 nm and E, 30 nm) and microgrooves (F, 60-μm wide microgrooves and 100 nm fibrils) by scanning electron microscopy. Scale bar: 10 μm (D), 5 μm (E), 500 μm (F).

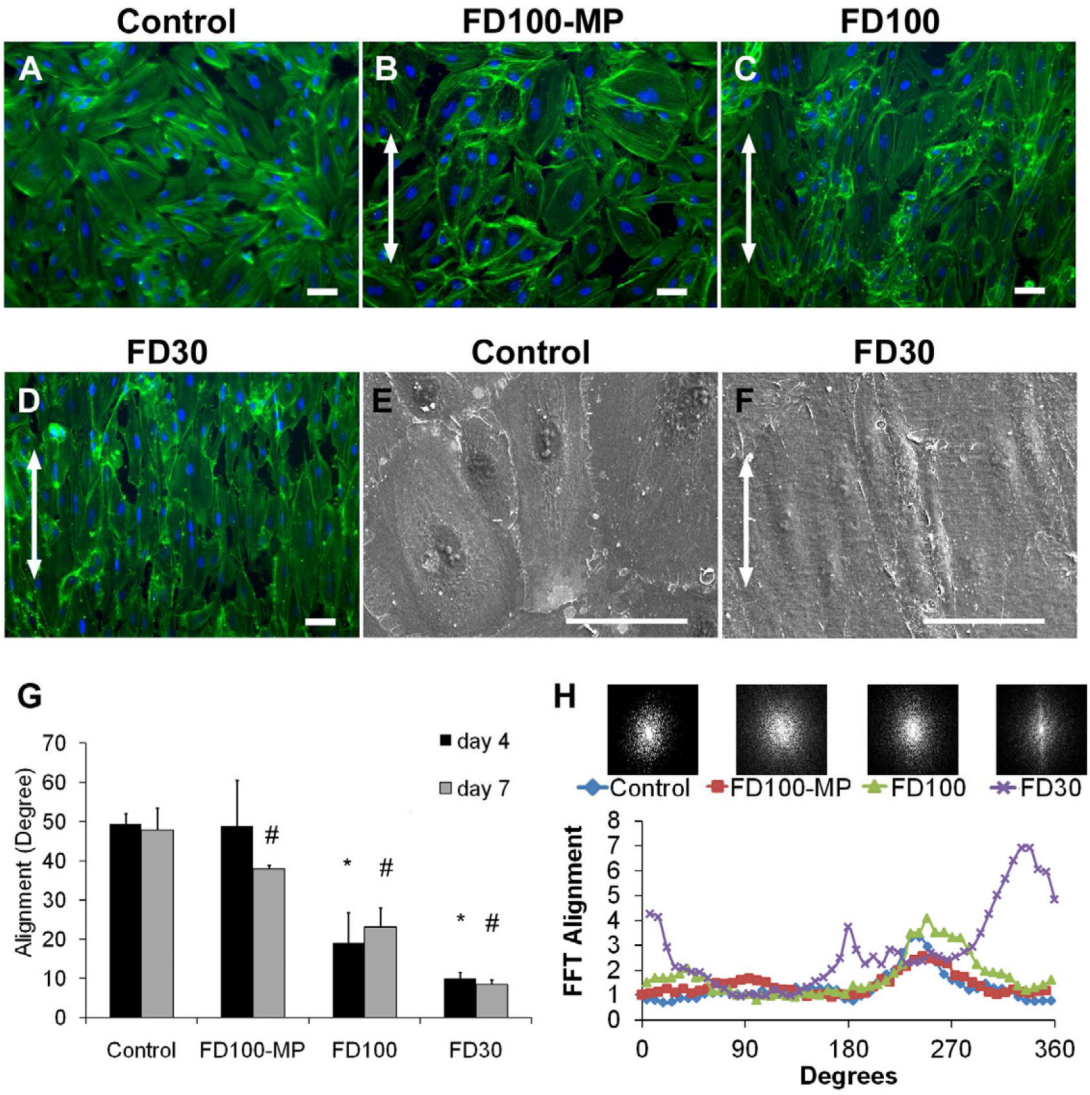

Fig. 2. EC morphology on aligned nanofibrillar membranes

Immunofluorescence staining with phalloidin (green) for cytoskeletal protein F-actin and Hoechst (blue) for nuclei after 7 days of cell culture on (A) collagen coated (control), (B) FD100-MP, (C) FD100, and (D) FD30 substrates. SEM images of (E) control and (F) FD30 samples. Arrows denote direction of collagen fibrils. G. Quantification of mean cell alignment, with respect to nanofibril direction. In this analysis, a value of 45° represents entirely random orientation of axes of cultured cells, whereas a value of 0° represents complete alignment of the cell s. H. Cell alignment after 7 days of cell culture was quantified by two-dimensional FFT analysis and depicted by alignment plots. Insets represent corresponding frequency plots. * Indicates statistically significant difference vs. control at day 4 ($p < 0.0001$); # indicates statistically significant difference vs. control at day 7 ($p < 0.0001$) ($n \geq 3$).

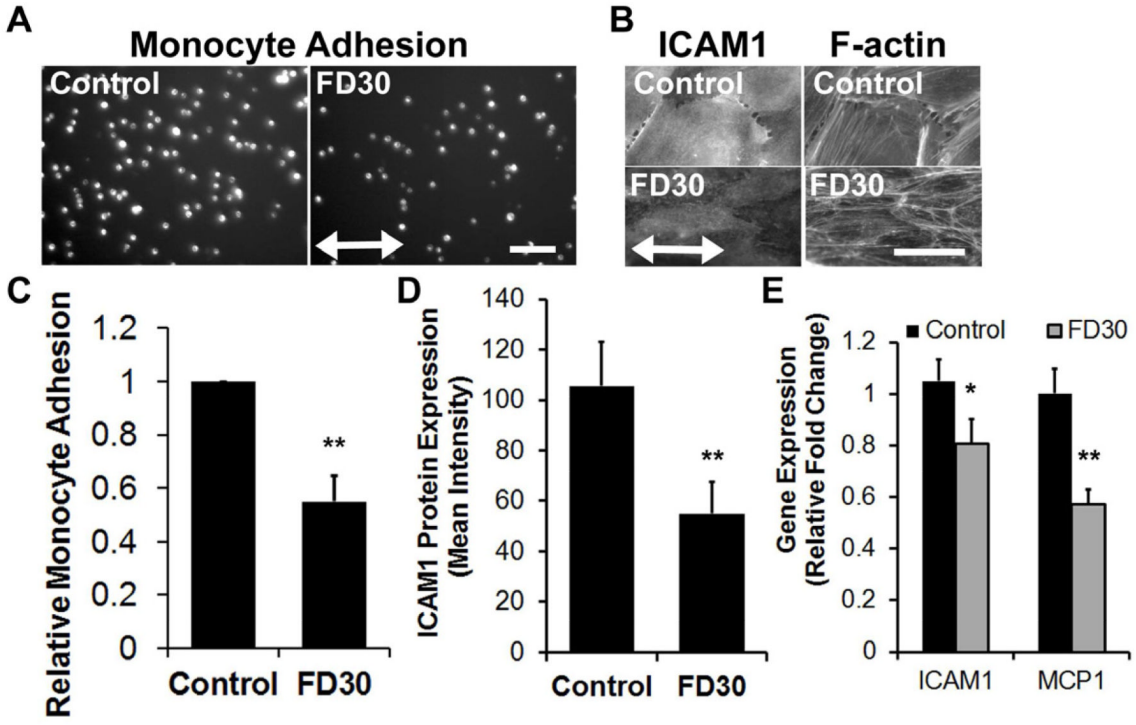

Figure 3. EC adhesiveness on oriented nanofibrillar collagen after TNFα treatment

A. Fluorescent images of U937 monocytes adhered onto ECs grown on control or FD30 substrates. B. Immunofluorescence staining of ICAM1 and corresponding F-actin staining on ECs cultured on control of FD30 substrates. C. Quantification of relative fold change monocyte adhesion on ECs grown on control or FD30 substrates (n=3). D. Quantification of mean ICAM1 protein expression based on intensity of immunofluorescence staining (n=5). E. Gene expression of ICAM1 and MCP1 on ECs on control or FD30 substrates (n=3). Arrow indicates direction of nanofibril direction. Scale bar, 100 m. *$p < 0.05$; **$p < 0.005$.

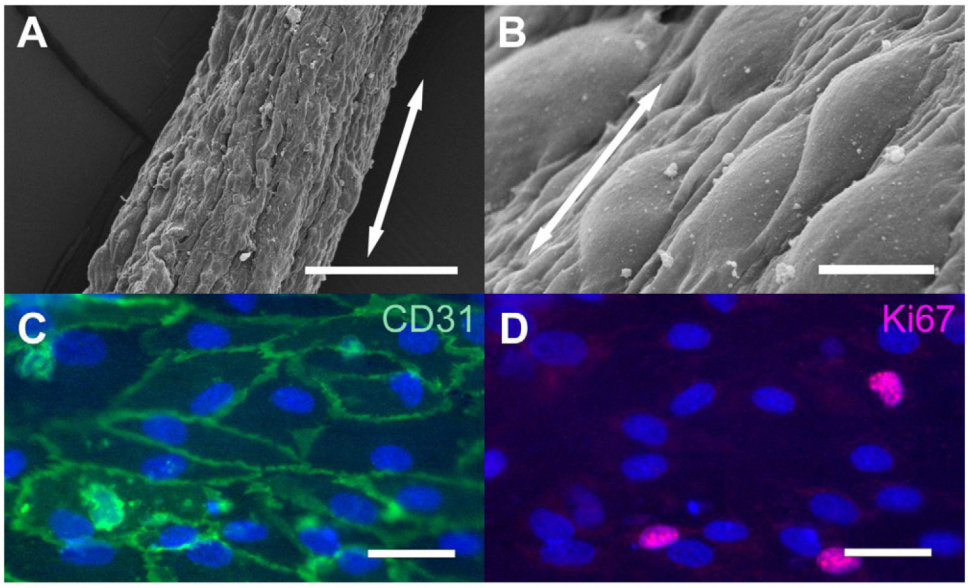

Fig. 4. Endothelial morphology and phenotype on FD30 collagen scaffolds

A-B) SEM of FD30 scaffolds at low (A) and high magnification (B). C. Immunofluorescence staining for endothelial marker CD31 (green) and nuclei (blue, Hoechst dye); D. Immunofluorescence staining for cell cycle marker, Ki67 (red) and nuclei (blue, Hoechst). Arrow denotes direction of collagen nanofibrils. Scale bar: 200 μm (A), 10 μm (B), 50 μm (C-D).

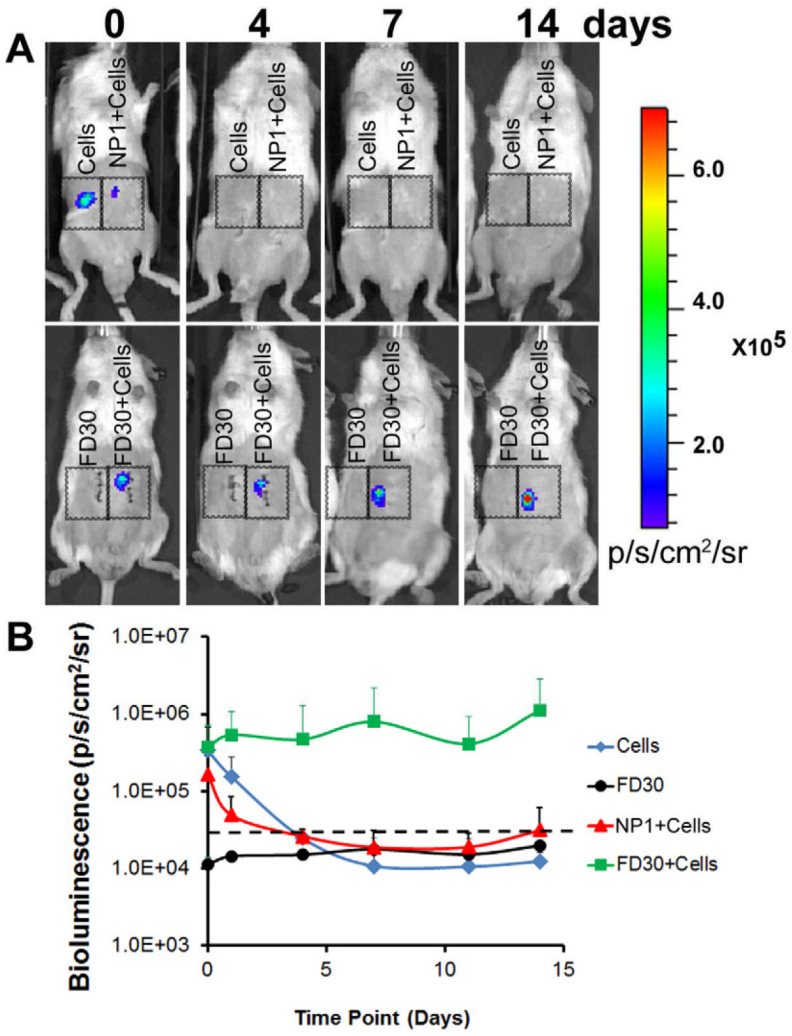

Figure 5. Aligned nanofibrillar collagen scaffold enhances endothelial survival after subcutaneous implantation

A. BLI reveals cell localization and survival of ECs when delivered as cells in DMEM (Cells), cells within a non-patterned scaffold (NP1+Cells), or cells within the FD30 scaffold (FD30+Cells). FD30 scaffold without cells (FD30) served as a negative control to establish background levels alone. B. Quantification of bioluminescence intensity. Dotted line indicates threshold for positive signal.

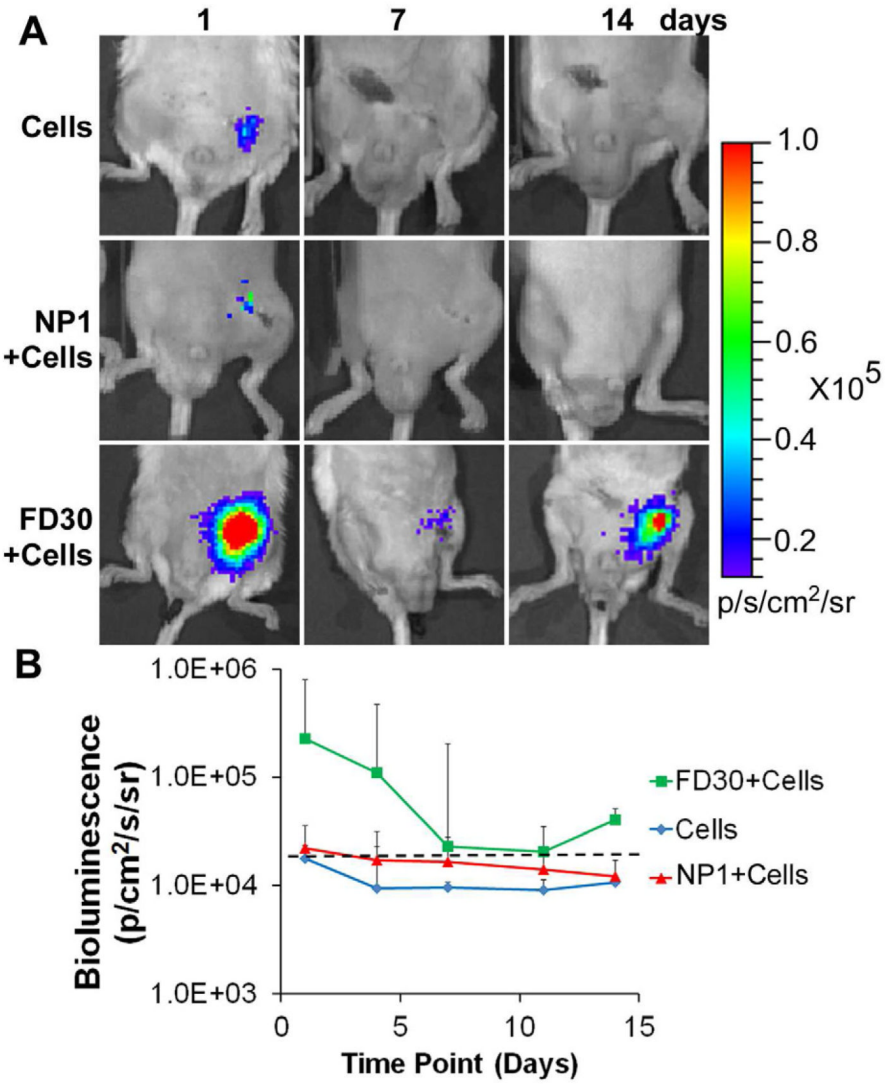

Figure 6. Aligned nanofibrillar collagen scaffold enhances endothelial survival after implantation into ischemic hindlimb

A. BLI reveals cell localization and survival of ECs when delivered alone (Cells), when seeded on non-patterned scaffold (NP1+Cells), or on FD30 scaffold (FD30+Cells). B. Quantification of bioluminescence intensity. Dotted line indicates threshold for positive signal.

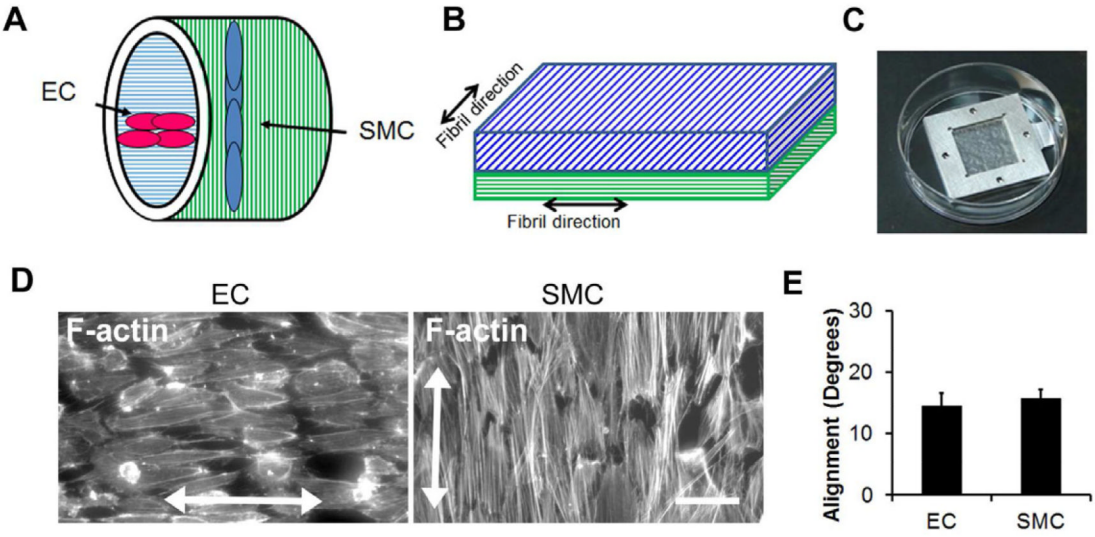

Figure 7. Application of oriented collagen nanofibers for fabrication of bilayered vascular grafts consisting of ECs and SMCs

A. Schematic of bilayered nanofibrillar vascular grafts (A) and bilayered membranes (B) that guide the assembly of ECs and SMCs orthogonal to one another. C. Metal frames were used for securing bilayered membranes. D. F-actin was used to visualize the alignment of ECs and SMCs oriented in orthogonal directions within the bilayered membranes. E. Quantification of cell alignment (n=3). Scale bar: 50 μm.